Buckling behavior of single-walled carbon nanotubes and a targeted molecular mechanics approach

Guoxin Cao and Xi Chen*

Columbia Nanomechanics Research Center, Department of Civil Engineering and Engineering Mechanics, Columbia University, New York, New York 10027-6699, USA

(Received 14 August 2006; revised manuscript received 27 September 2006; published 26 October 2006)

During the general (conventional) molecular mechanics (GMM) simulation of the buckling of single-walled carbon nanotubes (SWCNTs), the load is displacement controlled and the calculated critical buckling strain is very sensitive to the specific displacement increment and convergence threshold chosen in molecular dynamics (MD) simulations, which may have led to the contradictory and diverged results in the previous studies. In this paper, a targeted-molecular mechanics (TMM) simulation method is proposed to study the buckling behavior of SWCNTs under axial compression, bending, and torsion. Comparing with the GMM method, the TMM technique is independent of the displacement increment and thus the solution is converged. The critical buckling strain computed from the TMM is higher than that from the GMM under axial compression and torsion, and the TMM results are similar to the GMM results upon bending. The TMM result approaches to the intrinsic critical buckling strain of a perfect tube; in addition, the TMM significantly reduces the computational cost and thus may be more efficient to study larger systems with atomistic simulations.

DOI: 10.1103/PhysRevB.74.165422 PACS number(s): 65.80.+n, 61.48.+c, 61.50.Ah, 81.07.De

I. INTRODUCTION

Carbon nanotubes (CNTs) have been subjected to intensive research due to their excellent mechanical, electrical, and chemical properties. With the advance of experimental techniques, the buckling behaviors of the CNTs have been observed under large deformation which significantly reduces the structural integrity.[1–3] On the other hand, the CNT buckling is elastic, i.e., it can be completely recovered after unloading,[2,4,5] moreover, the physical properties such as the conductance of the CNTs can be significantly influenced by the occurrence of buckling or deformation, supported by both experiment and theoretical studies.[6–8] These facts may lead to potential applications of CNTs as the next-generation nanoelectronic devices (nanotransistors),[6] nanofluid components (nanovalves),[9] and reversible elements in nanoelectromechanical systems (NEMS) by transforming between the buckled state and normal state of the CNTs. Therefore, in view of both the mechanical integrity and application, it is important to understand the buckling mechanisms of the CNTs. The most important variable characterizing the buckling behavior is the critical buckling strain, measured at the onset of buckling.

Besides the development of the experimental investigations, both theoretical and numerical studies of the CNTs have been widely used to explore the buckling behavior of the CNTs, which can be divided into three main categories: (1) Atomistic simulation based on the molecular dynamics (MD),[10–20] with either classical or reactive empirical bond-order potential;[20] (2) continuum mechanics modeling where the CNTs are effectively modeled as continuous beams or thin shells with a fixed effective wall thickness, effective Young's modulus and Poisson's ratio;[11,19,21–26] (3) analytical modeling based on the molecular structural mechanics.[27,28] In a numerical simulation, individual factors can be turned on or off to explore their effects, thus as a first step, by studying the buckling behavior of a perfect tube under ideal loading modes, the numerical simulation may be used to unveil the intrinsic relationship between the critical buckling strain and tube geometrical parameters (e.g., length, radius, and chirality), and under several basic deformation modes (compression, torsion, bending), which is of fundamental value.

With the development of the more accurate (less empirical) forcefield and numerical algorithms, the MD simulations have been shown to play an important role in revealing the mechanical behavior of the CNTs. At present, although substantial MD studies have been carried out to explore the axial compressive buckling behaviors of the single-walled carbon nanotubes (SWCNTs), many of the findings are in contradiction with each other.[11–13,16] For axial compression, the onset of buckling refers to the critical configuration at which there is a sudden appearance of large lateral deflection (or bowing) of the tube to relieve the compression energy (since bending costs much less strain energy), and the critical buckling strain is the overall axial compression at buckle divided by the undeformed length of the tube. When the tube length/diameter aspect ratio is between 2 and 10, Buehler *et al.* reported that the critical buckling strain decreases with the decrease of tube length,[13] whereas Liew *et al.* found the opposite trend,[12] and Yakobson *et al.* argued length-independence.[11] Moreover, there is also a debate on the effect of chirality on the critical buckling strain.[12,16]

It should be noticed that in these conventional MD approaches carried out at or near 0 K, which are referred to as the general molecular mechanics (GMM) simulations in this paper, a displacement-controlled loading is applied to the atoms in both ends of the tube by using a specified displacement increment δ, until the desired overall axial compression (or bending/torsion angles in other applications) is reached. However, we have recently shown that the critical buckling strain of the SWCNTs under compression is very sensitive to the δ used in the GMM.[29] For example, for a tube with a fixed diameter, chirality, and length (which is moderately

long), a larger δ may cause a higher critical buckling strain than a smaller one. Whereas, for short tubes, the critical buckling strain randomly oscillates with the variation of displacement increments. These effects are more obvious for the nanotubes with smaller diameters. To overcome such uncertainty, we propose a targeted-molecular mechanics (TMM) simulation approach (inspired by the study of proteins[30]), which only optimizes the system once and thus not only induces the smallest possible uncertainty, but also significantly reduces the computation time. The details of the TMM method are elaborated below, after the discussion of the main limitation of the GMM.

In GMM simulations of axial compression, the strong influence of the displacement increment is related with the generation and accumulation of *geometrical defects*.[29] In most MD/MM programs, although it is desired that the net force acting on each atom is strictly zero after the potential optimization, such a goal would take forever to realize. Instead, the atomic system is regarded as being in an equilibrium state if all net forces acting on the atoms are smaller than a specified small value. Even though such convergence threshold (ξ) is very small and has a negligible influence on the system potential energy, after the potential optimization with finite ξ (typically in the range of 10^{-5} to 10^{-2} kcal/mole/Å), the coordinates of the atoms will be slightly different than their ideal positions if ξ is zero. In addition, in most MD/MM programs, the equilibrium state is a local minimum of the potential surface; thus, if the atomic system has many local minimums such as the SWCNT under axial compression, different initial atomic structures can lead to different final structures after the potential optimization.

Moreover, in the GMM the overall deformation is divided in to many small displacement increments. In order to reach a desired overall compression, the system needs to be optimized multiple times, and the optimized structure by the end of the current displacement increment is the initial structure of the next numerical increment. During axial compression, since the tube prefers to bow laterally in order to release its compression energy and reduce system energy, the lateral perturbation caused by geometrical difference is indispensable; thus, a very small geometrical difference in the initial structure may be enlarged after many times of optimization. Consequently, with the same overall compression but different displacement increments, they may cause non-unique solutions of the atomic coordinates of the optimized geometrical structure.

In this paper, the deviations of the computed atomic coordinates with respect to their ideal deformed positions (without the convergence threshold and at the global minimum of each optimization step) are referred to as the *geometrical defects* (or sometimes *defects* for simplicity). These geometrical defects are gradually accumulated from the geometrical differences generated during each numerical increment, until they become large enough to buckle the tube and relieve the compression energy.[29] The buckling behavior is very sensitive to perturbations.[31,32] At a critical point during axial compression, the accumulated geometrical defects will cause the tube axis to suddenly bow in the lateral direction and buckle, which is a preferred way to reduce the overall system energy. For a tube with moderate length, more loading steps are needed when a smaller δ is chosen, which accumulates to a larger geometrical defect and thus makes the tube easier to buckle.[29] We also note that these geometrical defects are fundamentally different than the real topological tube defects (e.g., the atomic vacancies or the Stone Wales defect), which are not considered in the current investigation.

The dependence of the critical buckling strain on the displacement increment used in the GMM simulations, which to our knowledge has not been discussed previously in the literature, is likely to be one of the reasons that has caused the aforementioned diverged and contradictory numerical results.[11–13,16] In view of the importance of a converged atomistic simulation of the buckling mechanisms of SWCNTs, we propose two basic questions:

(1) Besides the strong dependence of displacement increment on axial compression,[29] how does the critical buckling strain vary with the displacement increment used in GMM simulations of bending and torsion, such that we could better evaluate the buckling behaviors of tubes under bending and torsion?

(2) How to remove the effect of the displacement increment in atomistic simulations, such that the critical buckling strain becomes insensitive to the generation and accumulation of geometrical defects in MD simulations? Note that only after the removal of such effect, it becomes possible to relate the SWCNT geometrical parameters (e.g., the tube chirality, length and diameter) and the critical buckling strain through atomistic simulations.

In order to achieve the second goal, one obvious solution seems to reduce ξ to an even smaller value. However, as long as ξ is nonzero, regardless of how small it is, it will be shown that the adjustment of ξ cannot effectively reduce the generation and accumulation of geometrical defects in the GMM study. Moreover, by doing so the simulation time is significantly increased, which makes the GMM simulations much more computationally expensive.

With an affordable converging threshold, both the total number of loading increments and the maximum force acting on the carbon atoms during each increment need to be reduced as much as possible, such that the generation of geometrical defects becomes minimum in atomistic simulations. Inspired by this idea, a targeted-molecular mechanics (TMM) simulation method is introduced to study the intrinsic buckling behaviors of the SWCNTs, which only optimizes the system once and induces the smallest possible geometrical defects; similar idea has been applied to study the deformation of proteins.[30] By using the TMM approach, the buckling of SWCNTs under axial compression, bending, and torsion are investigated. The tube length, diameter, and chirality are varied and their effects are studied. The results are compared with those computed from the GMM, which shows the advantage and efficiency of the TMM method. The findings of this paper may help to develop a consistent strategy of analyzing the critical buckling strains under different loading modes, which are important for evaluating the CNT mechanical integrity and applying the buckled SWCNTs as NEMS components.

II. COMPUTATION METHODS

All atomistic calculations are carried out at 0 K with the molecular mechanics (MM) method, based on extensive con-

siderations in our recent work (including the avoidance of unrealistic loading rate and easier comparison with parallel continuum model).[29] The atomic interactions in the CNT system are modeled by using the condensed-phased optimized molecular potential for atomistic simulation studies (COMPASS) forcefield.[33] The initial structures of SWCNTs are assumed to be perfect, and the real topological tube defects, such as the atomic vacancies or the Stone Wales defect (i.e., pentagon and heptagon pair by rearrangement of the bonds), are not considered although they significantly reduce the buckling load. Note that while these topological defects are inevitable in a real tube employed in experiment, their overall effect may be represented by a fitting factor; a similar approach may be adopted for the effect of temperature or loading rate, which are currently under investigation. Nevertheless, by ignoring these factors in this paper, the fundamental and intrinsic relationship between the critical buckling strain and tube geometrical parameters can be explored, which may be subsequently revised by incorporating the fitting parameters to include the effects of topological defects, temperature, loading rate, etc.

With the increase of the quasistatic load, the system potential energy increases monotonically. Once buckle instability has initiated, the tube shape suddenly and significantly deviates from its expected deformation mode; at this instant, the total potential energy also sharply reduces. The critical buckling strain is characterized by the tube deformation at the critical configuration with respect to undeformed configuration, defined below with respect to three basic deformation modes (compression, bending, and torsion). For axial compression, buckle is characterized by the bowing of tube axis, whereas for bending and torsion, buckle is initiated by the snap kinks on tube surfaces at critical locations. Under various loading modes, the onset of buckling can be identified by either monitoring the abruptly varied tube shape, or by recording the sudden decrease of the tube potential energy.

A. The general molecular mechanics (GMM) simulations

The initial atomic structure of a SWCNT is optimized by the MM, such that the total potential energy is minimized and the net forces acting on the atoms are below ξ. In the GMM, a displacement-controlled loading is used with a specified displacement increment δ: (1) For axial compression, rigid body translations are applied to the atoms in both end layers of the SWCNT, such that the shape of both end layers remains circular with the original radius, and the distance between the two tube ends gradually reduces until a desired total compression Δ is reached. The total number of loading increments used in the simulation is Δ/δ. Such a displacement-controlled loading is easy to realize in practice and has been widely used.[11–13,16,29] (2) Upon pure bending, the atoms in both tube end layers are rigidly translated such that both end sections remain circular and are kept perpendicular to the deformed axis; the length of the deformed tube axis remains unchanged and its curvature is essentially uniform throughout bending.[10,11,14,19,34] (3) Under torsion, one end layer is fixed and rigid body rotation (with respect to the tube axis) is applied to the atoms in the other end layer of the SWCNT. Both tube ends remain the original circular shape, and the tube length is unchanged.[17,19]

During each displacement increment of the GMM, the end carbon atoms are first moved to their new positions, and then all other carbon atoms of the nanotube are driven to their new equilibrium positions by minimizing the system potential energy. There are two adjustable parameters in the simulations: δ and ξ. If the maximum net force acting on all atoms is less than ξ, then the system is considered as being in an equilibrium state.

B. The targeted molecular mechanics (TMM) simulations

In the TMM, the initial atomic structures are first optimized by the MM. Note that due to the many-body interactions, the atoms are not guaranteed to locate at their perfect cylindrical positions and small deviations (*initial geometrical imperfections*) are inevitable. Next, the loading is applied to *all* atoms in the system: for a given deformation magnitude, all carbon atoms are initially moved to their targeted positions, which are their ideal (assumed) deformed positions without buckle; next, with both end layers fixed, all other atoms are released and the whole system is optimized. The deformation magnitude is slowly increased by repeating this procedure until the buckle instability has occurred. In the TMM, the system is optimized only once during loading, and therefore the generated geometrical defects are the smallest. In addition, during the targeted movement, the distribution of atomic force and displacement are essentially uniform, which, during the subsequent optimization process, helps to generate less geometrical defects. In the TMM simulation, there is only one adjustable parameter, ξ.

For axial compression, the ideal (targeted) deformed tube shape is uniform compression along the axial direction to achieve the desired overall compression Δ. With varying Δ, the overall compression at the onset of buckling, Δ_{cr}, is identified from the deformed tube shape after optimization. The critical buckling (normal) strain is computed by $\varepsilon_{cr}^{compress} = \Delta_{cr}/L$, where L is the undeformed tube length; the same equation can be used in the GMM.

Upon bending deformation, the targeted deformed shape is that the tube axis changes to an arc (with a center angle, i.e., overall bending angle, θ). By ignoring the change of cross-sectional geometry, each layer of carbon atoms still keeps the original circular shape and remains perpendicular to the deformed axis. After all atoms are moved to their targeted positions, the system is optimized with both end layers fixed. By varying θ, the relationship between the total potential energy and the bending angle can be established. The bending angle at the onset of buckling is denoted by θ_{cr}. Upon buckling, the critical buckling (normal) strain computed from the TMM or GMM simulations is $\varepsilon_{cr}^{bend} = 1/2\,\theta_{cr} d/L$, where d is the tube diameter.

When the tube is twisting, the ideally deformed tube shape is that the tube axis remains straight and unchanged; with one end fixed, and the other tube end undergoes a twist angle of ϕ, and the remaining layers are twisted with an angle that is in proportion to their distance from the fixed

end. The critical twist angle ϕ_{cr} upon buckling can be found once instability occurs, and the critical buckling (shear) strain computed from the TMM or GMM is $\gamma_{cr}^{torsion} = 1/2\,\phi_{cr} d/L$.

C. Continuum shell modeling

The SWCNTs have been widely studied by using the continuum thin shell or beam models.[11–13,16,29] By fitting the continuum model from atomistic simulations of the SWCNTs under tension and bending, the effective wall thickness is $t \approx 0.066-0.089$ nm.[11,19,22,35] With respect to the different buckled shapes, the compressive buckling behaviors of the SWCNTs can be divided into three regions (which are confirmed from MD studies):[36] (1) the shell-like buckling behavior when L/d is small and/or d/t is large; (2) the transitional buckling behavior between the shell and the beam; (3) the beamlike buckling behavior when L/d is large and/or d/t is small. One of the most distinct features between the shell-like and beamlike buckling behaviors is the occurrence of snap buckles, which are absent in the buckled beams. With the monotonic variation of the tube length and/or diameter, it is expected that the buckling behavior can change from region (1) through (2) to region (3).

Closed form solutions for axial compressive buckling are available. For nanotubes displaying the beamlike buckling behaviors, by using beam theory, if $t^2 \ll d^2$, the critical buckling strain of a tube with both ends clamped can be described as[11,13]

$$\varepsilon_{cr\text{-}beam}^{compressi} = \frac{1}{2}(\pi d/L)^2. \tag{1}$$

The critical compressive buckling strain decreases as the inverse square of the beam length. On the other hand, when the nanotube is in the shell-like buckling region, the critical compressive buckling strain of an axishell is[11,13]

$$\varepsilon_{cr\text{-}shell}^{compress} = \frac{2}{\sqrt{3(1-\nu^2)}}\frac{t}{d} \approx 1.176\frac{t}{d}, \tag{2}$$

where the Poisson's ratio of the CNTs is ν=0.19. The critical compressive buckling strain of a perfect elastic thin shell is strictly independent of the tube length, and it is in general higher than that of a beam with the same section ratio. The critical compressive buckling strain of a tube in the transition region is between that of a shell and a beam.

The buckling behaviors of SWCNTs under bending and torsion deformations are more complicated. A beam does not buckle under bending or torsion. In addition, to our knowledge, there is no analytical solution for the critical buckling strain of a thin shell under pure bending.

III. NUMERICAL RESULTS

A. The general MM simulations

1. The critical buckling strain under axial compression

Figures 1(a) and 1(b) show the relationship between the critical buckling strain, $\varepsilon_{cr}^{compress}$, and the compressive displacement increment, δ, of different SWCNTs. The error bar

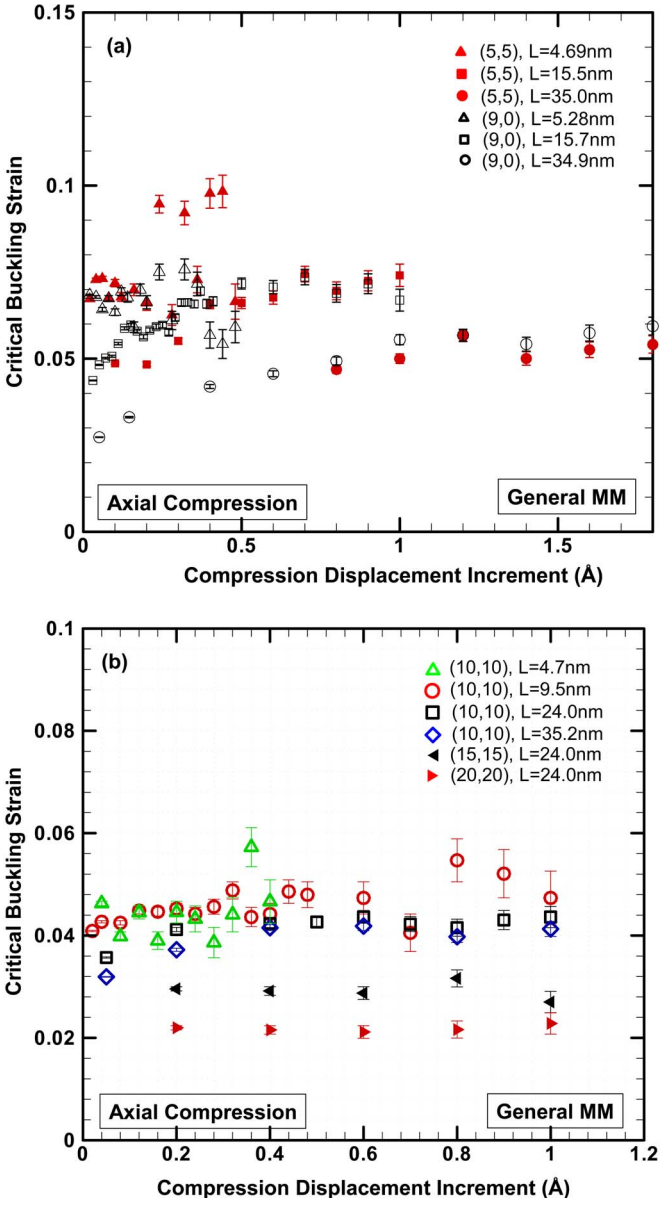

FIG. 1. (Color online) The effect of the compressive displacement increment on the critical buckling strain in the GMM simulations; the tubes with (a) smaller diameters and (b) larger diameters are under the axial compression.

equals to δ/L. For the (5,5) and (9,0) SWCNTs in the current range of tube length (L/d=7.0–50), the variation of $\varepsilon_{cr}^{compress}$ with changing δ can be more than 80% [Fig. 1(a)]. Whereas, for the larger (20,20) tubes, the difference of $\varepsilon_{cr}^{compress}$ with varying δ is reduced to about 10% [Fig. 1(b)]. In general, the $\varepsilon_{cr}^{compress}$ is very sensitive to δ used in the GMM, especially for smaller tubes. With the increase of d, $\varepsilon_{cr}^{compress}$ becomes less sensitive to δ. The reasons that cause these trends in the GMM have been discussed in Ref. 29, and briefly reviewed in Sec. I of this paper.

Figure 2 shows the effect of ξ on $\varepsilon_{cr}^{compress}$ for (5,5) tubes with lengths L=4.7 nm and L=9.5 nm. When ξ is varied from 10^{-5} to 10^{-2} Kcal/mole/Å, the increase of $\varepsilon_{cr}^{compress}$ can exceed 100% in the GMM simulations. In addition, when different values of ξ are used, the dependence of $\varepsilon_{cr}^{compress}$ on

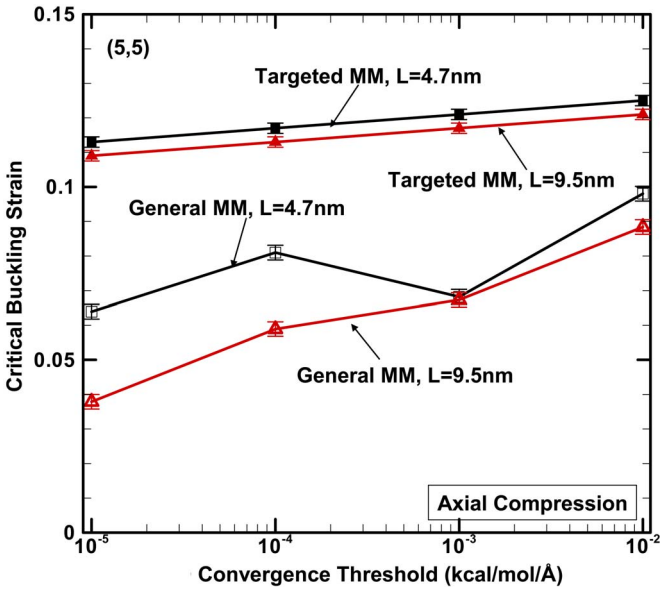

FIG. 2. (Color online) The effect of the MM convergence threshold (ξ) on the critical buckling strain under the axial compression in both the TMM and GMM methods, for (5,5) tubes with different tube lengths.

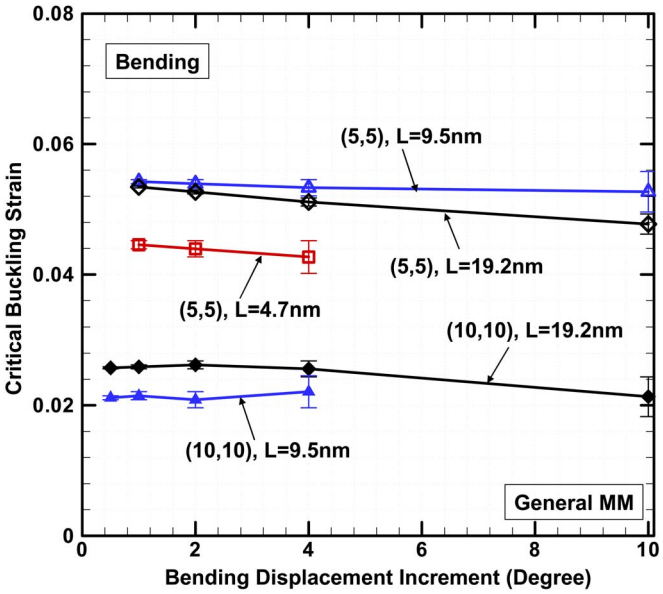

FIG. 3. (Color online) The effect of the bending displacement increment on the critical buckling strain under the bending deformation in the GMM method, for tubes with varying diameter and length.

tube length becomes uncertain (i.e., it is not clear whether longer tubes have smaller $\varepsilon_{cr}^{compress}$). Therefore, in the GMM, $\varepsilon_{cr}^{compress}$ is not only sensitive to δ, but also oscillates with ξ. The combination of these two factors may be the main reason to account for the contradictions in the previously reported GMM results of $\varepsilon_{cr}^{compress}$.

2. The critical buckling strain under bending deformation

Figure 3 shows that the relationship between the bending critical buckling strain, $\varepsilon_{cr}^{bending}$, and the bending displacement increment, $\delta\theta$, of the different SWCNTs. For both (5,5) and (10,10) tubes, $\varepsilon_{cr}^{bending}$ is insensitive to $\delta\theta$ for short tubes. For the longer (5,5) tube with $L=19.2$ nm, there is about 8% variation of $\varepsilon_{cr}^{bending}$ when $\delta\theta$ is increased from 1° to 10°; with the increase of the tube diameter, $\varepsilon_{cr}^{bending}$ becomes less sensitive to $\delta\theta$. The small reduction of $\varepsilon_{cr}^{bending}$ at a larger $\delta\theta$ may be related with the extra compression component introduced when $\delta\theta$ is large. The dependence of $\varepsilon_{cr}^{bending}$ on ξ is given in Fig. 4, for (5,5) tubes with $L=4.7$ nm and 9.5 nm. It can be readily seen that $\varepsilon_{cr}^{bending}$ is not sensitive to ξ for both tubes in the GMM method.

3. The critical buckling strain under torsion deformation

Figure 5 describes the relationship between the critical buckling strain under torsion, $\gamma_{cr}^{torsion}$, and the increment of twist angle, $\delta\phi$, of the different SWCNTs. For both (5,5) and (10,10) tubes, the increase of $\gamma_{cr}^{torsion}$ is about 20% with the increase of $\delta\phi$ from 1° to 10°. As the tube length increases, $\gamma_{cr}^{torsion}$ becomes less sensitive to $\delta\phi$. In addition, the effect of $\delta\phi$ on $\gamma_{cr}^{torsion}$ is not obvious when the tube diameter is changed. In Fig. 6, the relationships between $\gamma_{cr}^{torsion}$ and ξ are given for (5,5) tubes: when ξ is changed from 10^{-5} to 10^{-2} Kcal/mole/Å, the $\gamma_{cr}^{torsion}$ increases monotonically for about 35%, and such increment is slightly reduced for the longer nanotube.

B. The targeted MM simulations

1. The critical buckling strain under axial compression

Figure 7 shows the $\varepsilon_{cr}^{compress}$ calculated by the TMM for a variety of tube geometries that can be compared with the GMM in Fig. 1, where it can be seen that $\varepsilon_{cr}^{compress}$ calculated

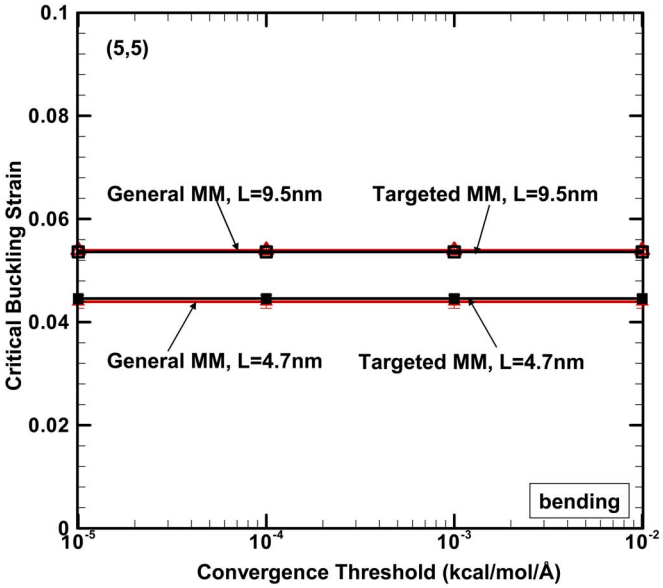

FIG. 4. (Color online) The effect of ξ on the critical buckling strain under the bending deformation in both the TMM and GMM methods, for (5,5) tubes with different tube lengths.

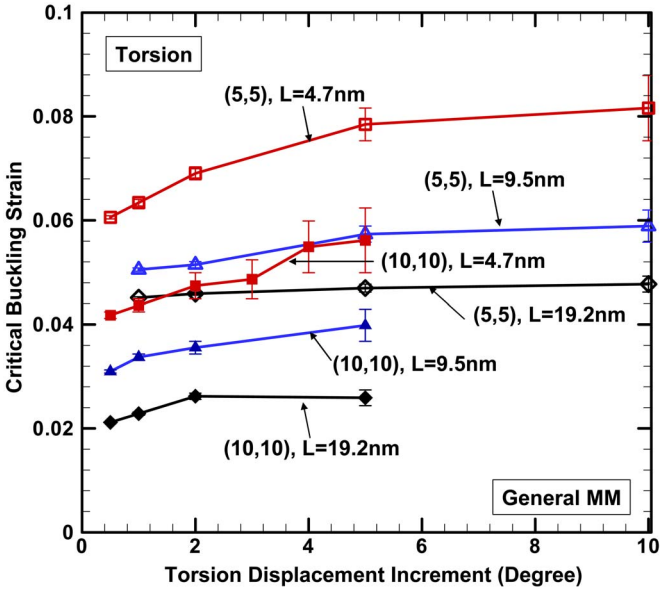

FIG. 5. (Color online) The effect of the bending displacement increment on the critical buckling strain under the torsion deformation in the GMM method, for tubes with varying diameter and length.

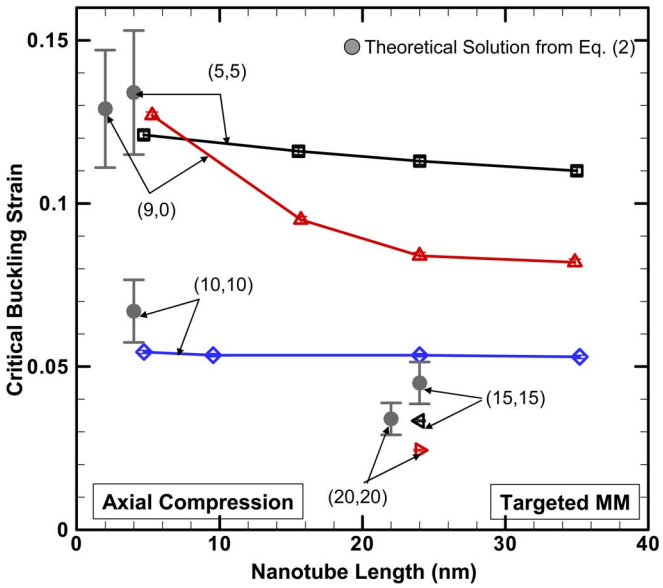

FIG. 7. (Color online) The critical buckling strain under the axial compression computed by the TMM method, for tubes with varying diameter and length. The theoretical results from Eq. (2) are also shown.

from the TMM is much higher than that from the GMM. For small diameter tubes, the maximum difference between two different methods can be more than 80%. For (5,5) tubes, the difference between the TMM and GMM increases with the increase of tube length; but for (9,0) tubes such trend is inversed. With the increase of tube diameter, however, $\varepsilon_{cr}^{compress}$ calculated from the GMM begins to reach the TMM solutions. For the (15,15) and (20,20) tubes, there is almost no difference between those two methods.

The effect of ξ on $\varepsilon_{cr}^{compress}$ calculated from the TMM is shown in Fig. 2. With the increase of ξ from 10^{-5} to 10^{-2} Kcal/mole/Å, the monotonic increase of $\varepsilon_{cr}^{compress}$ is only about 10%; such effect is much less than that in the GMM. In addition, the effect of ξ is almost the same for the two (5,5) tubes with different tube lengths; in other words, the relationship between $\varepsilon_{cr}^{compress}$ and the tube length is essentially independent of ξ.

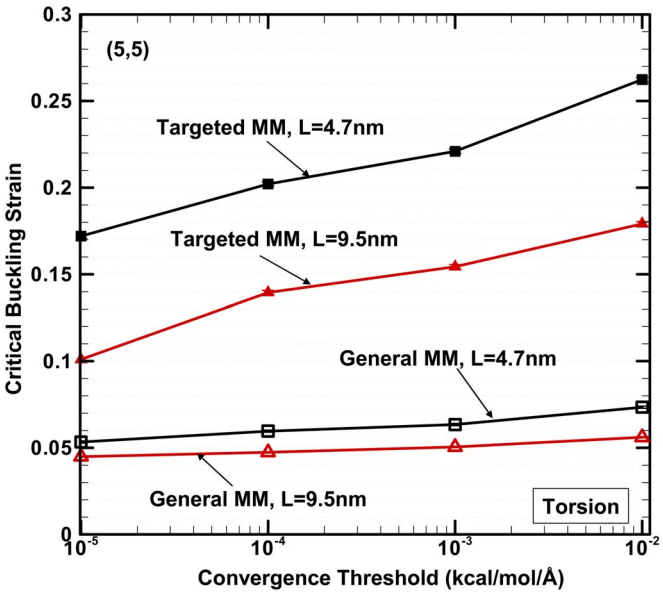

FIG. 6. (Color online) The effect of ξ on the critical buckling strain under the torsion deformation in both the TMM and GMM methods, for (5,5) tubes with different tube lengths.

2. The critical buckling strain under bending deformation

Figure 8 shows $\varepsilon_{cr}^{bending}$ calculated by the TMM for (5,5) and (10,10) tubes with different tube lengths. From the com-

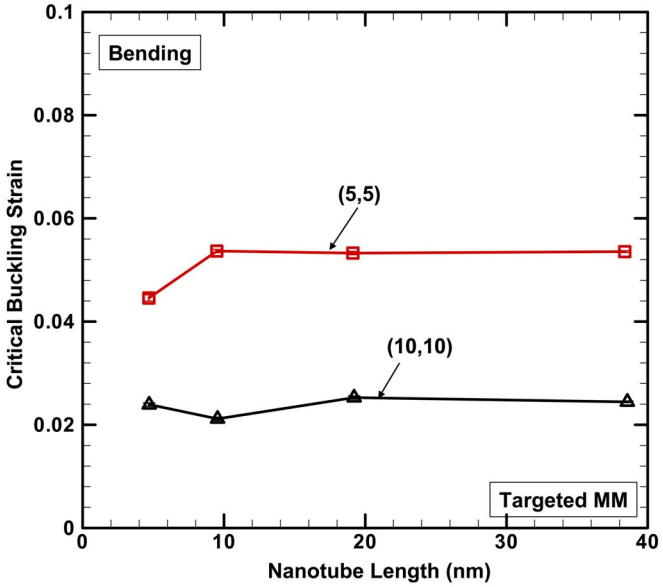

FIG. 8. (Color online) The critical buckling strain under the bending deformation computed by the TMM method, for tubes with varying diameter and length.

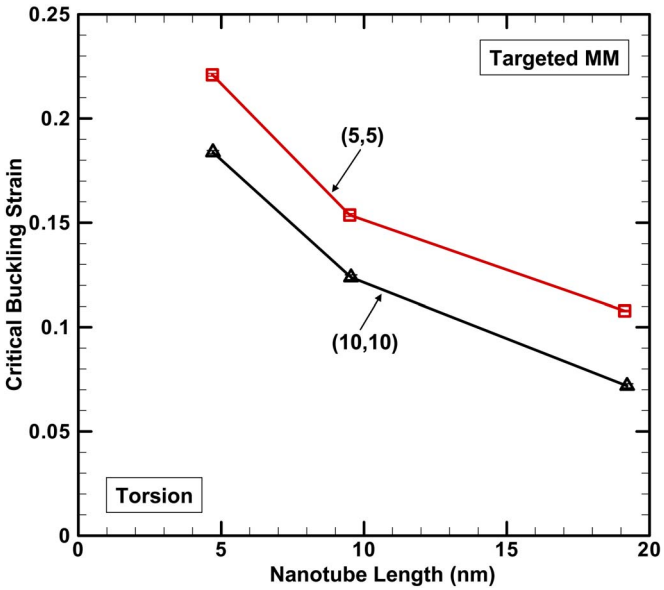

FIG. 9. (Color online) The critical buckling strain under the torsion deformation computed by the TMM method, for tubes with varying diameter and length.

parison between Figs. 3 and 8, it is apparent that with the decrease of $\delta\theta$, $\varepsilon_{cr}^{bending}$ calculated from the GMM begins to converge to the TMM solutions. Figure 4 also shows the effect of ξ on $\varepsilon_{cr}^{bending}$, for (5,5) tubes in the TMM simulations. The result is similar to that of the GMM simulations, i.e. $\varepsilon_{cr}^{bending}$ is essentially insensitive to the selected values of ξ.

3. The critical buckling strain under torsion deformation

Figure 9 shows $\gamma_{cr}^{torsion}$ calculated from the TMM simulations for (5,5) and (10,10) tubes with different lengths. By comparing Figs. 5 and 9, it is found that $\gamma_{cr}^{torsion}$ calculated from the TMM is much higher than that obtained from the GMM: for the short (5,5) tube with $L=4.7$ nm, the ratio between $\gamma_{cr}^{torsion}$ calculated from the TMM and that from the GMM (at the lowest $\delta\phi$ in Fig. 5) is about 3.7, and such ratio decreases to about 2.4 when $L=19.2$ nm; meanwhile, such ratio keeps increase with the increasing of the tube diameter. Figure 6 also shows the effect of ξ on $\gamma_{cr}^{torsion}$ for (5,5) tubes in the TMM. Comparing with the GMM, $\gamma_{cr}^{torsion}$ calculated by the TMM is more sensitive to ξ: with the increase of ξ from 10^{-5} to 10^{-2} Kcal/mole/Å, $\gamma_{cr}^{torsion}$ increases about 50% for the (5,5) tube with $L=4.7$ nm and about 80% for the (5,5) tube with $L=9.5$ nm, respectively.

IV. DISCUSSION: COMPARING THE RESULTS OBTAINED FROM TMM AND GMM UNDER DIFFERENT DEFORMATION MODES

A. The critical buckling strain under axial compression

The critical buckling strain, $\varepsilon_{cr}^{compress}$, calculated from the GMM is very sensitive to δ and ξ (Figs. 1 and 2). Therefore, it is very difficult to obtain the converged value of $\varepsilon_{cr}^{compress}$ and to identify a consistent relationship between the $\varepsilon_{cr}^{compress}$ and the SWCNT geometry (e.g., length, diameter, and chirality). In our recent work,[29] the effect of δ on $\varepsilon_{cr}^{compress}$ in the GMM simulations has been discussed (also refer to Sec. I), and the selection of reasonable δ to obtain the converged $\varepsilon_{cr}^{compress}$ has been proposed. By following such strategies, the effect of δ on $\varepsilon_{cr}^{compress}$ can be reduced yet it cannot be eliminated; moreover, such effect may be coupled with the effect of ξ to generate more inconsistent results (i.e. $\varepsilon_{cr}^{compress}$ oscillates in an unpredictable manner, c.f. Figs. 1 and 2).

The TMM method, which has eliminated the effect of δ, has clear advantages over the GMM approach on the calculation of $\varepsilon_{cr}^{compress}$. In addition, in the TMM simulations, the effect of ξ is significantly reduced (compare with the GMM). The buckled shapes of SWCNTs and the relationship between the tube strain energy and overall compression (before buckling) computed from the TMM and GMM methods are very similar. The typical buckled shapes and the strain energy-deformation relationships of SWCNTs computed by the GMM, under axial compression and with different geometries, can be found in Ref. 29. However, it is important to note that the $\varepsilon_{cr}^{compress}$ obtained from the TMM simulations (Fig. 7) is much higher than that from the GMM studies (Fig. 1)—is the $\varepsilon_{cr}^{compress}$ calculated from the TMM approach reasonable?

The continuum thin shell model has been successfully employed to simulate the buckling behavior of SWCNTs.[11,22–25] In addition, Ref. 29 showed that the theoretical solution of the $\varepsilon_{cr\text{-}shell}^{compress}$ derived from Eq. (2), is much higher than that obtained from the GMM simulations. We speculate that such difference is caused by the initial geometrical imperfections and the accumulation of geometrical defects discussed earlier: During a displacement increment of axial compression, the ideal movements of carbon atoms are along the axial direction, however, due to the small initial geometrical imperfections and the nonzero ξ, the carbon atoms are allowed to move slightly in the lateral direction which are different than their ideal positions (i.e., *geometrical differences*), which may cause a very small deviation of the tube axis from its ideal straight position (i.e., *geometrical defects*), and thus generate a small bending moment and bending strain energy. Since the strain energy upon compression is much higher than that of bending (or bowing),[37] the system would substantially reduce its potential energy if the tube deformation could deviate from pure compression and transit to bending deformation. Therefore, as long as the small bending component is generated, the corresponding small geometrical difference will be carried over into the next loading increment. With the increased number of displacement increments, the bending energy will become larger and so does the lateral deflection of the tube axis (which will lead to the accumulation of the geometrical defects); when such defects become large enough, the tube buckles at a critical load.[29]

The above assumption may be further verified by comparing the TMM solution and the continuum theory [Eq. (2)]; the results are shown in Fig. 7. The error bar of the theoretical solution represent the $\varepsilon_{cr\text{-}shell}^{compress}$ calculated within the tube wall thickness range found in the literature,[11,19,22,35] $0.066\ \text{nm} < t < 0.089\ \text{nm}$ (note that the theoretical solution is length independent). The relatively small difference between

the continuum theory and the TMM solution can be attributed to the initial geometrical imperfections; whereas, the difference between the GMM and TMM solutions (Fig. 2) comes from the geometrical defect generated within the large number of loading increments in the GMM. After removing the effect of the geometrical defects on $\varepsilon_{cr}^{compress}$, the TMM solution is much closer to the continuum thin shell theory than the GMM solution, i.e., the TMM solution is approaching to the intrinsic critical buckling strain of an initially perfect tube. Therefore, it is apparent that the TMM can be more effectively used to investigate the critical buckling strain of a SWCNT under axial compression.

B. The critical buckling strain under bending deformation

The buckled shapes of SWCNTs upon bending and the evolution of the bending strain energy (before buckling) are almost identical for the same tube in the GMM and TMM simulations. The typical buckled shapes and the strain energy-bending angle relationships for tubes with different geometry can be found in Ref. 34. In the GMM, $\varepsilon_{cr}^{bending}$ increases only slightly with the decrease of $\delta\theta$ (Fig. 3), and the result is also insensitive to ξ (Fig. 4). In addition, $\varepsilon_{cr}^{bending}$ calculated from the TMM is very close to the GMM result at very small values of $\delta\theta$: These characteristics are very different than the situations under axial compression.

Upon bending in GMM, the curvature of the tube axis will gradually increase until the tube buckles. Unlike axial compression where the tube axis remains straight, during bending, the tube axis updates to a new curvature after every loading increment. By doing so, the geometrical defects generated from the last increment are released by the new adjustment of the tube axis, and thus it is not transferable. In other words, there is not much reduction of strain energy with defect accumulation in bending, thus it is not preferred. This explains why $\varepsilon_{cr}^{bending}$ does not decrease with the increased number of numerical increments, as well as the small difference between the TMM and GMM approaches. Moreover, in the GMM simulation, a larger $\delta\theta$ causes more unevenly distributed forces on the carbon atoms with an axial compressive component, which leads to a larger difference between the deformed tube axis and the ideal pure bending axis (a perfect arc) after the potential optimization, and therefore causes the tube easier to buckle.

Under bending, the TMM still holds advantage over the GMM method, since it can remove the effect of $\delta\theta$ in GMM (although not very large). More importantly, the TMM takes much less time to simulate the bending buckling behavior than the GMM, since the difference between the targeted SWCNT unbuckled structure and the snap buckled tube is small.

C. The critical buckling strain under torsion deformation

Similar to the case of compression in the GMM, $\gamma_{cr}^{torsion}$ increases with the increase of $\delta\phi$ (Fig. 5). In addition, $\gamma_{cr}^{torsion}$ is also sensitive to ξ (Fig. 6). Upon twisting, just like compression, the small geometrical defects generated in each loading increment will be transferred to the next increment, which finally accumulate to a critical value that is sufficient to cause buckle. During torsion, since both tube ends and the tube axis are fixed, the release of the geometrical defects generated in the previous increment is not allowed. Therefore, a larger $\delta\phi$ will cause a higher $\gamma_{cr}^{torsion}$ because the larger $\delta\phi$ requires fewer loading increments and generates less geometrical defects. We also note that from continuum mechanics, $\gamma_{cr}^{torsion}$ is expected to be larger than the critical normal strain, $\varepsilon_{cr}^{compress}$ or $\varepsilon_{cr}^{bending}$—such trend agrees with the findings of this paper although a direct comparison is unavailable, since the buckling also depends on the stress gradients and boundary conditions under the different loading modes.

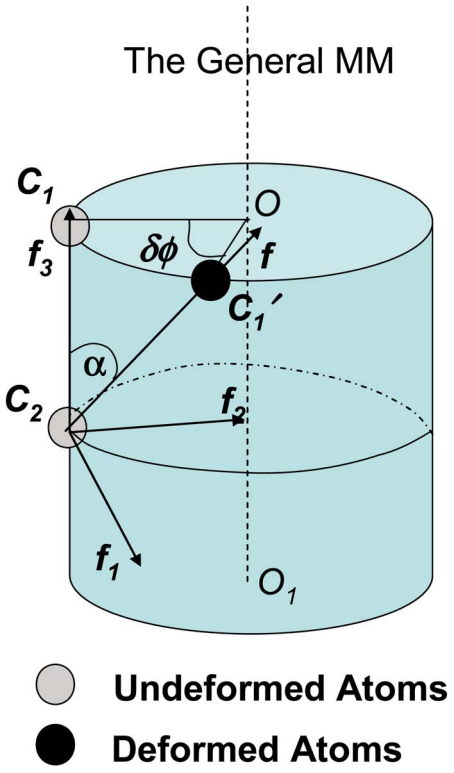

FIG. 10. (Color online) The schematic of a tube under the torsion deformation in the GMM method.

The $\gamma_{cr}^{torsion}$ calculated from the TMM is much larger than that obtained from the GMM study—such behavior is distinct from the results under axial compression and bending. For any deformation mode, the differences between the GMM and TMM solutions are caused by: (1) the geometrical defects generated within each displacement increment, which is due to the nonuniformly distributed forces acting on the atoms; (2) the accumulation of the geometrical defects.

Under the axial compression (for both GMM and TMM), the net force acting on each atom is lying essentially within the cylindrical plane. However, the case is different for the tube under the torsion. Figure 10 shows the schematic of a tube under torsion deformation in the GMM simulation. Within a particular displacement increment, when the atom C_1 is rotated with $\delta\phi$ and then fixed, the original C_1-C_2 bond changes to C_1'-C_2 and the net force, f, is acting on the atom C_2 and along the C_1'-C_2 direction. The force f can be decomposed into several components: f_1 along the circumferential

direction, f_2 along the radial direction, and f_3 along the axial direction. The atom C_2 will be driven to its new position by the pulling force f, and after the equilibrium optimization, the force between these two atoms will be reduced almost to zero after the atom C_2 reaches to its new equilibrium position. Among the three components, the f_2 component is along the radial direction which causes the extra radial perturbation—the most sensitive perturbation to cause the buckling of a thin shell.[32] Therefore, under torsion deformation, the geometrical defects generated in each loading increment are larger (compared to that in axial compression and bending), which cause the prominent difference between the GMM and TMM solutions.

V. CONCLUSION

In this paper, a targeted-molecular mechanics (TMM) method is introduced to simulate the critical buckling strain of SWCNTs under several basic deformation modes: axial compression, bending and torsion. The comparison is made between the results obtained from the general molecular mechanics (GMM) simulation and the TMM approach.

The main differences between the TMM and GMM include: (1) there is only one loading increment in the TMM, which can effectively remove the accumulation of the geometrical defects during the GMM, and thus remove the effect of the displacement increment which is a main source of uncertainty in the GMM approach; (2) in the TMM, the net forces acting on all atoms are more uniformly distributed and smaller than those in the GMM simulations. The above differences cause the different critical buckling strains under the different loading modes.

Under axial compression, $\varepsilon_{cr}^{compress}$ calculated from the TMM is much higher than that obtained from the GMM, and the results are close to the theoretical solution. The numerical results have verified the role of the geometrical defects accumulated during the loading of the GMM, which causes the large difference between the $\varepsilon_{cr}^{compress}$ calculated from the GMM and the continuum model. The small difference between the TMM and theory is due to the initial geometrical imperfection. Furthermore, the TMM approach is much less sensitive to ξ than that in the GMM study. Combined, these factors make the TMM solution approaching to the intrinsic critical buckling strain of the SWCNT, and thus more attractive.

Upon bending, $\varepsilon_{cr}^{bending}$ calculated from the TMM is very close to its GMM counterpart (at a very small $\delta\theta$). In addition, the $\varepsilon_{cr}^{bending}$ calculated from both methods are not sensitive to ξ, which is due to the absence of the geometrical defect accumulation under bending.

When the tube is subjecting to twisting deformation, $\gamma_{cr}^{torsion}$ calculated from the TMM is much higher than the GMM. The out-of-plane perturbation induced during the GMM torsion may cause large geometrical perturbation within one displacement increment. In addition, $\gamma_{cr}^{torsion}$ calculated from both methods are sensitive to ξ in the MD simulations.

We finally remark that the TMM simulations hold obvious advantages over the GMM simulations in studying the critical buckling strain of the SWCNTs under different deformation modes. The TMM method is much more efficient in terms of computation time and it reproduces the post-buckling shape of the GMM simulation, making it even more attractive. Therefore, the proposed targeted-MM simulations have the potential to advance the understanding of the buckling behaviors of the SWCNTs.

ACKNOWLEDGMENTS

This work is supported in part by NSF CMS-0407743 and in part by Columbia University Academic Quality Fund.

*Corresponding author. Email address: xichen@civil.columbia.edu

[1] H. Dai, J. H. Hafner, A. G. Rinzler, D. T. Ccbert, and R. E. Smalley, Nature (London) **384**, 147 (1996).
[2] P. Poncharal, Z. L. Wang, D. Ugarte, and W. A. de Heer, Science **283**, 1513 (1999).
[3] S. Iijima, C. Brabec, A. Maiti, and J. Bernholc, J. Chem. Phys. **104**, 2089 (1996).
[4] M. R. Falvo, G. J. Clary, R. M. Taylor, V. Chi, F. P. B., Jr., S. Washburn, and R. Superfine, Nature (London) **389**, 582 (1997).
[5] T. W. Tombler, C. W. Zhou, L. Alexseyev, J. Kong, H. Dai, L. Liu, C. S. Jayanthi, M. J. Tang, and S. Y. Wu, Nature (London) **405**, 769 (2000).
[6] H. W. C. Postma, T. Teepen, Z. Yao, M. Grigoni, and C. Dekker, Science **293**, 76 (2001).
[7] J. Q. Lu, J. Wu, W. Duan, F. Liu, B. F. Zhu, and B. L. Gu, Phys. Rev. Lett. **90**, 156601 (2003).
[8] J. Wu, J. Zang, B. Larade, H. Guo, X. G. Gong, and F. Liu, Phys. Rev. B **69**, 153406 (2004).
[9] M. Grujicic, G. Cao, B. Pandurangana, and W. N. Royb, Mater. Sci. Eng., B **117**, 53 (2005).
[10] S. Iijima, C. Brabec, A. Maiti, and J. Bernholc, J. Chem. Phys. **104**, 2089 (1996).
[11] B. I. Yakobson, C. Brabec, and J. Bernholc, Phys. Rev. Lett. **76**, 2511 (1996).
[12] K. M. Liew, C. H. Wong, X. Q. He, M. J. Tan, and S. A. Meguid, Phys. Rev. B **69**, 115429 (2004).
[13] M. Buehler, Y. Kong, and H. Gao, J. Eng. Mater. Technol. **126**, 245 (2004).
[14] P. Liu, Y. W. Zhang, C. Lu, and K. Y. Lam, J. Phys. D **37**, 2358 (2004).
[15] M. B. Nardelli and J. Bernholc, Phys. Rev. B **60**, R16338 (1999).
[16] T. Ozaki, Y. Iwasa, and T. Mitani, Phys. Rev. Lett. **84**, 1712 (2000).
[17] Y. Shibutani and S. Ogata, Modell. Simul. Mater. Sci. Eng. **12**, 599 (2004).
[18] D. Srivastava, C. Wei, and K. Cho, Appl. Mech. Rev. **56**, 215 (2003).
[19] X. Chen and G. Cao, Nanotechnology **17**, 1004 (2006).

[20] A. Garg and S. B. Sinnott, Phys. Rev. B **60**, 13786 (1999).
[21] A. Pantano, M. C. Boyce, and D. M. Parks, Phys. Rev. Lett. **91**, 145504 (2003).
[22] A. Pantano, D. M. Parks, and M. C. Boyce, J. Mech. Phys. Solids **52**, 789 (2004).
[23] C. Q. Ru, J. Mech. Phys. Solids **49**, 1265 (2001).
[24] M. Arroyo and T. Belytschko, Phys. Rev. Lett. **91**, 215505 (2003).
[25] X. Q. He, S. Kitipornchai, and K. M. Liew, J. Mech. Phys. Solids **53**, 303 (2005).
[26] C. Q. Ru, Phys. Rev. B **62**, 9973 (2000).
[27] T. Chang and H. Gao, J. Mech. Phys. Solids **51**, 1059 (2003).
[28] C. Y. Li and T. W. Chou, Mech. Mater. **36**, 1047 (2004).
[29] G. Cao and X. Chen, Nanotechnology **17**, 3844 (2006).
[30] Y. Kong, Y. Shen, T. E. Warth, and J. Ma, Proc. Natl. Acad. Sci. U.S.A. **99**, 5999 (2002).
[31] J. W. Hutchinson and W. T. Koiter, Appl. Mech. Rev. **23**, 1353 (1970).
[32] M. Stein, AIAA J. **6**, 2339 (1968).
[33] H. Sun, P. Ren, and J. R. Fried, Comput. Theor. Polym. Sci. **8**, 229 (1998).
[34] G. Cao and X. Chen, Phys. Rev. B **73**, 155435 (2006).
[35] K. N. Kudin, G. E. Scuseria, and B. I. Yakobson, Phys. Rev. B **64**, 235406 (2001).
[36] G. Cao and X. Chen, J. Mater. Res. **21**, 1048 (2006).
[37] S. P. Timoshenko and J. M. Gere, *Theory of Elastic Stability* (McGraw-Hill, New York, 1961).